Optimistic Verifiable Training by Controlling Hardware Nondeterminism

Megha Srivastava [1] **Simran Arora** [1] **Dan Boneh** [1]

Abstract

The increasing compute demands of AI systems, such as training foundation models, has led to the emergence of services that train models on behalf of clients lacking necessary resources. However, ensuring correctness of training and guarding against potential training-time attacks, such as data poisoning and backdoors, poses challenges. Existing works on verifiable training largely fall into two classes: proof-based systems, which struggle to scale due to requiring cryptographic techniques, and "optimistic" methods that consider a trusted third-party auditor who replicates the training process. A key challenge with the latter is that hardware nondeterminism between GPU types during training prevents an auditor from replicating the training process exactly, and such schemes are therefore non-robust. We propose a method that combines training in a higher precision than the target model, rounding after intermediate computation steps, and storing rounding decisions based on an adaptive thresholding procedure, to successfully control for nondeterminism. Across three different NVIDIA GPUs (A40, Titan XP, RTX 2080 Ti), we achieve exact training replication at FP32 precision for both full-training and fine-tuning of ResNet-50 (23M) and GPT-2 (117M) models. Our verifiable training scheme significantly decreases the storage and time costs compared to proof-based systems, carving a pathway for a more efficient solution for verifiable training of large foundation models.

1. Introduction

We are currently in the "large-scale era" of machine learning (ML), where the exciting capabilities of modern AI systems, such as large foundation models (FMs), have required a dramatic increase in training compute needs (Sevilla et al., 2022). In turn, several model training services, such as Replicate, OpenAI's Finetuning API, Together AI, Amazon Sagemaker, MosaicML Training, and Gensyn, have been created to support clients who lack the resources to train a model themselves. However, these services require clients to place a significant degree of trust in them to train the model correctly, without introducing a training-time attack such as data poisoning or undetectable backdoors (Wan et al., 2023; Goldwasser et al., 2022). How can we help a client, such as an individual or a small company, hold the service provider accountable in case of misbehavior during training?

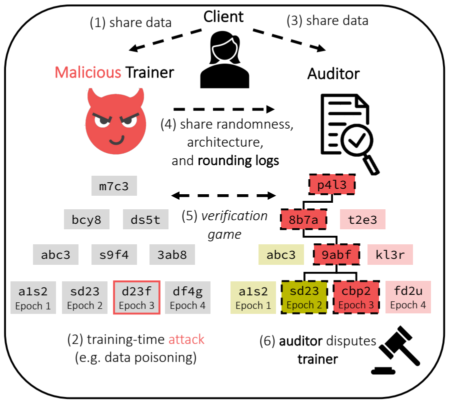

Figure 1. Overview of our verifiable training scheme, based on Teutsch & Reitwießner (2019). After an auditor challenges a trainer on behalf of a client, they train the model themselves, storing weights in a Merkle tree, and enter a binary search procedure to identify the exact steps of the dispute. We show how to account for hardware nondeterminism so that the auditor and trainer can use different GPUs, expanding the pool of potential auditors to any party capable of performing the training task.

One possibility is for the trainer to provide the client with a cryptographic proof that the model was trained according to the specification. However, proof-based systems require cryptographic techniques that are inefficient and cannot scale to the complexity of real-world tasks such as FM training. For instance, recent work based on zero-knowledge proof systems for verifiable *inference*, a much simpler task than training, requires more than 8 minutes to generate proofs for only 20 images (Liu et al., 2021). Thus, practical proof-based methods for verifiable training have only been implemented for simple tasks such as logistic and linear regression (Garg et al., 2023; Ames et al., 2022).

[1]Computer Science Department, Stanford University. Correspondence to: Megha Srivastava <megha@cs.stanford.edu>.

An alternative "optimistic" approach is to consider a trusted third-pary auditor, such as a non-profit organization, that has sufficient computing resources to perform the training task, even if not at the bandwidth of a service provider (Figure 1). When a client suspects foul play, they can ask the auditor to challenge the trainer by training the model using the auditor's own compute, and demonstrate that the trainer did not train correctly. Based on the evidence required from the auditor (i.e. the precise timesteps model training diverged, as shown in Figure 1), the client can then choose to refuse the trainer's model, pursue legal action against the trainer, or even dispute a potentially corrupt auditor if the client deems such evidence as invalid. This protocol can be efficiently carried out using techniques from the literature on verifiable computing, such as the "verification game" method of Teutsch & Reitwießner (2019), which uses an interactive binary-search procedure to identify the exact intermediate computation step (e.g., training epoch) where the two parties diverged.

Unfortunately, this approach breaks under nondeterminism during training: two models trained on different GPU types, even with same data order and random seed, learn different weights (Figure 2). Therefore, simply comparing the auditor's and trainer's model weights is not robust due to errors from nondeterminism (Jia et al., 2021; Thudi et al., 2022; Fang et al., 2023). We address this limitation by asking: can the trainer provide any information to the auditor that eliminates nondeterminism? We first observe that nondeterminism results from error accumulation in floating-point (FP) operations – a matrix-vector multiply can result in different outputs on different GPUs. If these errors are confined to only the higher precision bits, then one could train using a *higher* precision (e.g., FP32) than the target precision of the model (e.g., FP16), and round back to the target precision. However, outputs can occasionally straddle the rounding boundary, causing the trainer and auditor to diverge, and obtain entirely different models. We propose a solution where the trainer records rounding directions for some intermediate computations so that auditor will perfectly match the trainer.

We then use this strategy to adapt the verification game from Teutsch & Reitwießner (2019) for verifiable training, where an efficient Merkle tree (Merkle, 1988) data structure stores model checkpoint hashes. To determine if training was performed correctly, the auditor compares the root hash of their Merkle tree with the trainer's. If they do not match, the two parties enter an interactive binary search game to identify the exact training step of the dispute. This procedure holds both parties accountable: an auditor cannot simply claim that a model was improperly trained, but should convince a third-party (e.g., the public, or a judge) by showing at what point during training the trainer misbehaved. Our verifiable training scheme can scale to tasks such as full training of ResNet-50 (23M parameters) and finetuning of GPT-2 (117M parameters), significantly outperforming existing methods with respect to both time and storage cost (e.g., over **140** x for GPT-2), and eliminates non-determinism errors.

Concretely, our contributions include: (1) A method to eliminate nondeterminism between two parties training the same model on different GPU types; (2) A verification scheme based on this method, which stores model weights in a Merkle tree for efficient comparison between a trainer and auditor; (3) Experiments showing the ability of our scheme to scale to large (e.g., ResNet-50, GPT-2) between three NVIDIA GPUs (A40, Titan XP, RTX 2080 Ti); (4) Methods to reduce the storage cost of our approach, including an adaptive threshold mechanism to reduce the amount of rounding decisions logged; and (5) Comparisons with existing methods, including proof-based systems, that highlight the improved storage and time efficiency of our method, which is implemented entirely within `pytorch`.

2. Related Works

Without any verifiable training scheme, significant trust is placed in the trainer, leaving a client vulnerable to many different attacks, such as "poisoning" of data samples to cause undesirable behavior (e.g., generating unsafe text (Carlini et al., 2023; Koh et al., 2021; Wan et al., 2023)) and planting backdoors triggered by certain inputs (Goldwasser et al., 2022). Therefore, training ML models in trusted environments has been an exciting direction explored by many researchers. One line of work consists of proof-based systems, where a proof of correctness (for a desired specification) is provided using cryptographic techniques such as succinct non-interactive arguments (SNARKs) (Micali, 1994; Bitansky et al., 2012; Lee et al., 2020; Liu et al., 2021; Garg et al., 2023; Kang et al., 2022). However, even the most recent proof-based systems for verifiable *training* suffer extreme latency, such as 22 minutes for training VGG-11 on one batch of 16 data inputs (Abbaszadeh et al., 2024), and have primarily been developed for simpler models (e.g., logistic regression) that are less likely for a client to delegate out training for in the first place (Garg et al., 2023; Ames et al., 2022). Meanwhile, an alternative solution of training models in a trusted execution environment (TEE), such as NVIDIA's H100 "Confidential GPU", incurs a performance penalty due to the cost of running inside a TEE (Dhanuskodi et al., 2023). Furthermore, clients lose all security guarantees if an attacker can extract the attestation key from even one GPU (Nilsson et al., 2020; Bulck et al., 2018).

Our approach is most similar to proof-of-learning protocols, which consider a trusted 3rd party that compares checkpointing during the course of training with the original training sequence (Jia et al., 2021). However, such methods not only incur high storage cost by requiring model weights to be stored frequently, but are non-robust due to errors from training nondeterminism. Several works have shown that proof-of-learning protocols can be spoofed and fail to verify correctness in several important contexts (Fang et al., 2023; Kong et al., 2023; Thudi et al., 2022). Although Choi et al. (2023) recently proposed a verification procedure that is immune to several known proof-of-learning attacks, their method is not only limited to supervised learning algorithms, but also based on an assumption that models temporarily overfit data during training, which may not always hold true.

GPU Nondeterminism: Prior work has investigated software patches for deterministic training, for instance by enforcing FP accumulation ordering, at a significant cost to efficiency (Jooybar et al., 2013; Defour & Collange, 2015; Chou et al., 2020; TensorFlow, 2021; Zhuang et al., 2021). While these options address deterministic computation on a *single* GPU architecture, achieving deterministic results across multiple GPU architectures remains challenging (Crane, 2018a; NVIDIA, 2022). We control hardware nondeterminism across GPUs in order to design an efficient and reliable verifiable training scheme. However, our method's impact extends beyond verifiable training, as nondeterminism can have several negative consequences including bias, reproducibility, and downstream effects on ML pipelines (Zhuang et al., 2021; Crane, 2018b; Srivastava et al., 2020).

3. Set-Up: The Verification Game

Our method for verifiable training is based on the interactive verification game proposed by Teutsch & Reitwießner (2019) in the context of blockchains. The core idea is to resolve a dispute between a challenger, in our case the $\mathrm{auditor}$, and a solver, in our case the $\mathrm{trainer}$, for an expensive computation (e.g., model training). In order for the $\mathrm{auditor}$ to take any meaningful action (e.g., pursue legal action), they need to prove the exact source of the dispute (e.g., training time-step where an attack occurred). If we can save model weights at different time steps into a compact data structure such as a Merkle tree, then identifying the source of disagreement can be done efficiently using binary search (Merkle, 1988). More precisely, the verification game consists of the following parties:

1. $\mathrm{trainer}$, who has putatively trained a model according to a client's specifications. In our example, this is a service provider with sufficient compute power to train a model.
2. client, who receives a model from the $\mathrm{trainer}$ and approaches an $\mathrm{auditor}$.
3. $\mathrm{auditor}$, who officially challenges the $\mathrm{trainer}$ on behalf of a client. This is a 3rd-party that has sufficient resources but does not necessarily provide training as a service. The client can choose several auditors to audit the $\mathrm{trainer}$'s model.
4. judge: Sometimes a judge may need to arbitrate a legal claim. The judge can perform small computations (e.g., one training epoch), but can examine the $\mathrm{auditor}$'s claims and enforce a penalty against either the $\mathrm{trainer}$, for incorrect training, or the $\mathrm{auditor}$, for a false alarm.

When the $\mathrm{trainer}$ is approached by an $\mathrm{auditor}$, they would need to share training parameters, model architecture, and randomness, as shown in Figure 1. The $\mathrm{auditor}$ would then replicate the training process, storing model weights in a Merkle tree at the same checkpointing interval as the trainer (ever leaf node in a Merkle tree is a hash of the data and every non-leaf node is a hash of its children). The main loop of the verification game starts when both parties have the root of their respective Merkle trees. If training was performed correctly, then the $\mathrm{trainer}$'s root should match the $\mathrm{auditor}$'s. Otherwise, a binary search procedure is performed, where the $\mathrm{auditor}$ iteratively descends the Merkle tree until it identifies two consecutive leaf nodes, i and $i+1$, where the hash at i matches that of the $\mathrm{trainer}$, but the hash at leaf $i+1$ does not. This identifies the point in the computation of the dispute.

This interactive verification game requires the cooperation of the $\mathrm{trainer}$. If the $\mathrm{trainer}$ refuses to share the value at a certain node of their Merkle tree within a given time frame, they can be considered to have failed the audit. Additionally, the $\mathrm{trainer}$ and $\mathrm{auditor}$ use a Merkle tree to store model weights, requiring far less storage than prior work, if correct training produces identical weights (and identical hash values).The problem is that training nondeterminism leads to weight divergence, and causes this verification game to always fail, so we seek to prevent divergence in training.

4. The Nondeterminism Challenge

Although there are user-side controls for forcing deterministic operations within a single GPU architecture , these controls do not prevent nondeterminism between GPU architectures (e.g., NVIDIA H100 and V100), where trained models can have similar aggregate performance (e.g., accuracy) yet yield very different predictions, as shown in Figure 2 (Crane, 2018a; NVIDIA, 2022). There are three main sources of nondeterminism between GPU types:

1. Floating-Point Arithmetic: Computers represent real values using integer and FP representations, typically the IEEE 754 standard (Figure 5). There is a tradeoff between the approximation fidelity and the # of bits used to represent the real values. The chosen precision controls the representable numerical range (e.g., 32-bit FP values can represent values between $1.17549435e-38$ and $3.40282347e+38$). Because computers round to representable FP values, changing the order in which FP numbers are accumulated can change the resulting sum (Kahan, 1965;

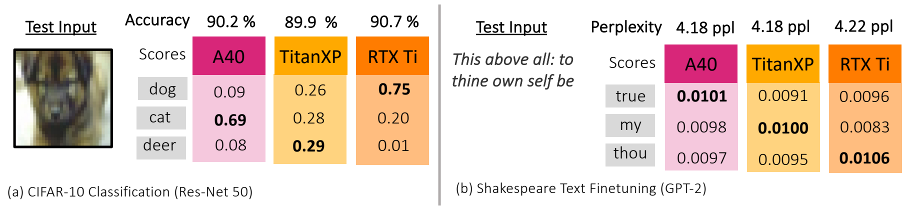

Test Input

Accuracy	90.2 %	89.9 %	90.7 %
Scores	A40	TitanXP	RTX Ti
dog	0.09	0.26	**0.75**
cat	**0.69**	0.28	0.20
deer	0.08	**0.29**	0.01

(a) CIFAR-10 Classification (Res-Net 50)

Test Input

This above all: to thine own self be

Perplexity	4.18 ppl	4.18 ppl	4.22 ppl
Scores	A40	TitanXP	RTX Ti
true	**0.0101**	0.0091	0.0096
my	0.0098	**0.0100**	0.0083
thou	0.0097	0.0095	**0.0106**

(b) Shakespeare Text Finetuning (GPT-2)

Figure 2. Even after ensuring the same software version, random seed, and use of deterministic algorithms via library flags, training nondeterminism persists between three GPU types.

Whitehead & Fit-Florea, 2011). Over the course of the many operations during training, this can lead to a large difference in the end result between the trainer and auditor.

2. Parallel Computation: In a GPU, a single operation (called a *kernel*) is executed by thousands of threads in parallel. GPUs contain a set of *streaming multiprocessors* (SMs), which run the *thread blocks* required for the kernel. At the hardware level, these blocks are divided into *warps* that are assigned to the available cores. Because different GPUs have a different number and size of compute units, applications partition arithmetic workloads (e.g., batch matrix multiplies) differently to achieve high performance (NVIDIA, 2022), thus changing the order of FP operations.

3. Memory Hierarchy and Variable Delays: The time taken for memory access by each thread depends on the physical location of the data, which can create variable delays (Jooybar et al., 2013; Defour & Collange, 2015; Chou et al., 2020). The GPU memory hierarchy consists of large amounts of high bandwidth memory (HBM) and small amounts of fast SRAM memory, and maintains an L1 and L2 cache to improve access times. The caches sizes and access times differ across GPU architectures, which affects warp scheduling. For instance, an NVIDIA A100 has 192KB / 40 MB of L1/L2 cache memory, while the H100 has 256KB / 50MB (NVIDIA, 2023).

To compute primitives such as GEMMs ($D = A \cdot B + C$), the workhorse of machine learning, GPUs split the work of computing the tiles of D across a thread block (NVIDIA, 2023), resulting in nondeterminism across GPUs that any robust verifiable training method would need to control.

5. Method Overview

5.1. Accumulation Errors Start at Higher Precision Bits

Our key idea is that if nondeterminism of training between GPU types occurs due to FP operations, then any error will initially be introduced in the lower bits. Suppose that both trainer and auditor train at a *higher* FP (e.g., $b_{tr} = 64$) precision than the client's target model precision (e.g., $b_m = 32$) and then periodically *round* (e.g., $b_r = 32$) after intermediate computation steps (e.g., a convolution layer). One might hope that this will "erase" the errors due to nondeterminism, and prevent them from accumulating. Unfortunately, simply rounding to the nearest FP32 after each computation during training is insufficient for determinism. The problem is due to rounding errors that straddle the *rounding boundary*. Consider Case A in Figure 3, which shows a divergence in the output of a computation using FP64 on two different GPUs. Because the outputs of GPU 1 and 2 are on different sides of the boundary, rounding to the nearest FP32 results in different values, introducing error.

What if the trainer records their rounding choice (e.g., up, down, none) for every intermediate computation? The auditor could then copy the trainer's choice, and therefore round to the exact same value and successfully control for nondeterminism. However, the auditor should not copy the trainer's behavior for every output (see Cases B & C, Figure 3). If a computation output on GPU 1 is too close to the rounded value, then it is possible that GPU 2 is also close in distance but from the opposite direction. In this case, the auditor should ignore the trainer's choice. We therefore need to introduce a threshold τ under which the trainer does not record their rounding choice.

Our method requires upper bounding the divergence d_{div} between any two different GPUs for any intermediate computation f (i.e. difference in outputs for the same input). Let ϵ_b represent the distance between two FP32 values, after rounding to b_r bits of the mantissa (Figure 5) and controlling for the exponent. We need to select b_r and τ such that $d_{div} < \epsilon_{b_r}$ and $d_{div} < 2\tau$ (Figure 3). Because the set of possible FP numbers is finite, there exist optimal bounds for b_r and τ. In practice, we find that $b_r \leq 32$ and $\tau > 0.25 \cdot \epsilon_{32}$ are sufficient for standard intermediate computations in neural network training (e.g., convolution, layer norm) in FP64. We study different values for b_r in Section 6.

5.2. Primitives

We assume both trainer and auditor train models using the IEEE-754 standard FP numbers (Figure 5). Besides requiring read and write disk I/O operations, we define the following functions:

1. $\mathsf{rnd}_{b_r}(x)$: rounds input x to the nearest FP up to b_r bits of the mantissa, as shown in Figure 5.
2. $\mathsf{log}(x, b_r, \tau, f)$: logs to file f a logging direction c, which

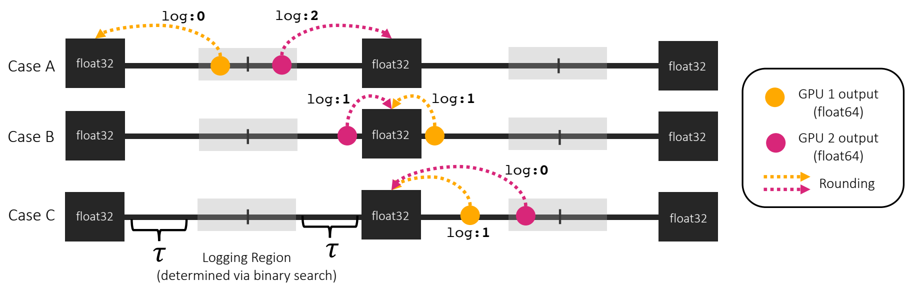

Figure 3. Divergence between outputs on two different GPUs (in FP64) for a given function and input can result in different rounding choices when rounding to the nearest FP32. We only wish to log rounding decisions for Case A, where the auditor should copy the trainer's rounding choice in order to reach the same value. This requires defining a logging region, determined by a threshold τ,

is either 0 (down), 1 (ignore), or 2 (up) depending on threshold τ and rounding amount b_r, as shown in Algorithm 4.

3. $\mathsf{rev}(x, b_r, c)$: reverses rounding of input x based on logging direction c. If $x < \mathsf{rnd}_{b_r}(x)$ & $c = 0$, then return x rounded to the nearest float *below* x with b_r precision. If $x > \mathsf{rnd}_{b_r}(x)$ & $c = 2$, then return x rounded to the nearest float *above* x with b_r precision. Otherwise, do not correct.
4. $\mathsf{threshold}(l, b_r, b_{tr})$: identifies the optimal threshold to log rounding directions (0 or 2) instead of 1, which the rev function ignores, based on the binary search procedure in Section 5.4.
5. $\mathsf{hash}_{\mathsf{sha256}}(\theta)$: creates a SHA-256 hash of provided model weights θ (in b_m precision).
6. $\mathsf{tree}(\mathit{leaf}_1, \mathit{leaf}_2 ..., \mathit{leaf}_n)$: create a Merkle tree where each *leaf* node is the output of $\mathsf{hash}_{\mathsf{sha256}}(\theta)$ for model weights θ at a given checkpoint, with a checkpointing interval k (Merkle, 1988).

5.3. Training and Auditing

The trainer's task begins when a client approaches them with dataset D, training specifications (epochs E, loss function loss, etc.), and a requested model precision b_m.The trainer can then choose a training precision $b_{tr} > b_m$, a rounding amount $b_r \leq b_m$, and a checkpointing interval k to periodically store small $\mathsf{hash}_{\mathsf{sha256}}(\theta)$ of model weights θ in a Merkle tree, for efficient comparison with an eventual auditor. Then, as detailed in Algorithm 1, the trainer can perform training as normal, but after every intermediate computation (e.g., convolution) perform the rnd_{b_r} operation on each output. Rounding is applied to computations in both the forward and backward passes. Finally, either using a fixed threshold τ or a layer-specific optimal τ from the threshold function described in Section 5.4, the trainer applies log, which logs rounding choices *only for the computations an auditor should copy*. The output of the algorithm includes a rounding log file F and the root of the Merkle tree which, along with the shared randomness R and all training parameters, the trainer can share with any trusted third-pary auditor who challenges them.

After a client approaches them, the auditor initiates the verification game described in Section 3. To avoid penalty, the trainer must cooperate by sharing the rounding amount b_r, randomness R used in training (e.g., a pseudo-random number generator), the checkpointing interval k, and set of rounding logs F. The auditor then follows the training procedure and corrects their rounding choice (e.g., up or down) to match those logged in F using the rev operation, as detailed in Algorithm 2 (Appendix). By correcting each rounding mismatch during the course of training, the auditor is able to prevent nondeterminism errors from accumulating. Therefore, the auditor can store the $\mathsf{hash}_{\mathsf{sha256}}(\theta)$ of model weights θ in a Merkle tree at interval k, knowing that if training was done correctly, the model weights should be identical to the trainer's at any timestep. The output of Algorithm 2 is the root of the auditor's Merkle tree, which they can use to compare with the trainer's root.

5.4. Reducing storage cost

Logging rounding decisions for every neural network layer output during training incurs a large baseline storage cost, and is our main limitation. For dataset D, batch size B, training epochs E, and model layers L_θ, the upper bound on the total storage cost for verifiable training with our method is:

$$\text{storage cost (B)} = |D| \times E \times B \times \left(\sum_{l=1}^{L} o_{l,f} + \sum_{l=1}^{L} o_{l,b}\right) \quad (1)$$

where $o_{l,f}$ and $o_{l,f}$ represent the size of outputs of the forward pass and backward pass of layer l. Note that the log entries do not need to be kept around in the RAM and can be written straight to the disk. Moreover, this cost is a one-time cost incurred by the trainer, who in our context is likely to be a powerful commercial provider with access to such storage capacity. Furthermore, as we later show in Section 6, for models with many linear layers like Transformer-based language models (e.g., GPT-2), where parameters significantly outnumber intermediate computations, this storage cost is significantly smaller than alternative approaches that require saving model weights (Jia et al., 2021). Nevertheless, we now describe our method for reducing storage cost by (i) efficiently encoding rounding logs and (ii) adaptive selection of the threshold τ to reduce the storage costs.

Efficient Encoding: Each log entry is a value from the set $0, 1, 2$, as opposed to the FP model weights. We pack sub-sequences of five log entries into a single byte via a fast GPU-based radix-3 to radix-2 conversion, yielding 1.6 bits/entry storage that is close to the best possible packing of 1.58 bits/entry, and yields a 77% storage reduction relative to naively storing one log entry per byte.

Adaptive Threshold: Recall that we need to select a threshold τ that controls for whether the trainer logs a rounding choice, or instead logs `1` which the auditor ignores. The more one can increase τ, the more `1` values are recorded, which can make rounding logs more compressible (due to long sequences of `1`s). Furthermore, it is possible that the divergence d_{div} between outputs on two different GPUs, given the same input, is function-specific. For example, while convolution requires several matrix multiplications that might result in a large FP accumulation error, normalization operations are unlikely to result in large d_{div}, and a larger τ can be applied. We develop an efficient algorithm (Algorithm 3 in the Appendix) to find the optimal value for τ given a particular layer and data of output values that led to different rounding choices between any two GPUs (e.g., Case A in Figure 3). For a given rounding amount b_r and training precision b_{tr}, the algorithm performs a binary search between $\tau = 0.25 \cdot \epsilon_{32}$ (our upper bound on the d_{div} between two GPUs for any function) and $\tau = 0.5 \cdot \epsilon_{b_r}$ (the rounding boundary). By performing this procedure for the different intermediate computations in a model, the trainer can hope to better compress the rounding log F.

Merkle Tree Storage: Storing SHA-256 hashes of model weights during training in a Merkle tree creates an efficient mechanism for the verification game described in Section 3, with negligible storage requirements. The audit ends when either the trainer withdraws, the auditor confirms that training was performed correctly, or the auditor can present paths to the two leaves of their Merkle tree where divergence starts, providing evidence to dispute the trainer.

6. Empirical Results

We evaluate our verifiable training method on the two large-scale models listed below with all possible trainer and auditor pairs across NVIDIA GPUs A40, TITAN Xp, and RTX 2080 Ti (see Appendix B). In Section 6.2, we compare our method with recent proof-based systems.

1. **ResNet-50**: We train (from random initialization) ResNet-50 (23M) on CIFAR-10 with dataset size 50K & batch size B=64. Test accuracy = 90.7% after 100 epochs training on Titan RTX Ti.
2. **GPT-2**: We finetune GPT-2 (117M) on a corpus of Shakespeare text with dataset size 1.1M tokens, batch size B=8, and sequence length 64. Perplexity = 4.22 after 1 epoch training on Titan RTX Ti.

Figure 2 shows that nondeterminism due to GPU architecture exists for both tasks. While we can repeatedly obtain identical results across training runs on the same GPU architecture, training on different GPU architectures results in fundamentally different models.

6.1. Implementation and Findings

We implement our verifiable training method entirely on top of the `pytorch` framework, with `torch` version 1.13.1 and CUDA version 11.7. The intermediate computations we apply $\mathsf{rnd_b}$ to are layers (e.g., `torch.nn.Conv2D`) in the model's computation graph. Rounding-related operations (rnd and rev) either using casting or FP functions (e.g., `torch.nextafter`) that can run on the GPU, thus having little impact on computational speed. Because we observed that the `torch.randn` operation used for dropout in GPT-2 is non-deterministic for long inputs (even for the same seed, see Appendix I), we implement our own dropout as our method requires shared randomness R.

Successful control for non-determinism: Our method completely eliminates non-determinism between full training runs of both for both the ResNet-50 training and GPT-2 fine-tuning tasks across all possible trainer and auditor pairs between the A40, Titan XP, and RTX 2080 Ti GPUs. As Figure 4 shows, standard FP32 training results in an increasing divergence (l2-distance of weights) between models on different GPUs over the course of training. Furthermore, we show the simple approach of training in FP64 and rounding to FP32 after every intermediate computation, but without the auditor correcting rounding decisions with rev, fails to mitigate this issue. Only our method, in which the auditor follows the rounding decisions ($b_r = 32$) made by the trainer for every intermediate computation, eliminates non-determinism and persists over time. Our implementation, which requires disk I/O during training to store the rounding decisions, results in a small increase in training time for the trainer (1.2-1.4x) and auditor (1.3-1.7x) using a non-optimized, protoype implementation (Table 4). We report the storage requirements of our method in Table 1, showing that our efficient encoding scheme reduces the size of the trainer's rounding logs by 77%, relative to naive logging. Because the Merkle tree stores 32-byte SHA-256 hashes, its overall size (KBs) and creation time are negligible and not reported. Finally, we show that decreasing the rounding amount b to values even as low as 26 has little effect on model performance (we observe no change in accuracy, so report test loss), but increase training time (Figure

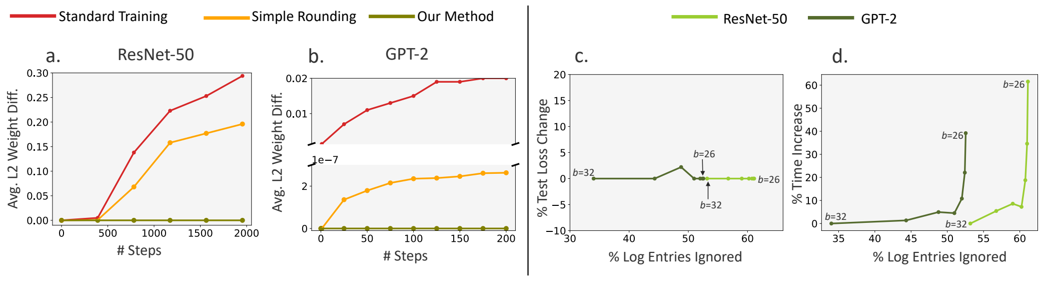

Figure 4. We successfully control for nondeterminism between GPU types for both ResNet-50 (a.) and GPT-2 (b.) tasks, while standard training and simple rounding without performing rev corrections result in model divergence over the course of training. Stronger rounding has minimal affect to model performance (c.), but at the cost of increasing time for trainer (d.).

Table 1. Efficient encoding reduces storage requirements by 77%, and rounding to $b = 26$ improves the compression further between 5-20% (values reported for 1 step of training). The original proof-of–learning protocol from Jia et al. (2021) requires storing 2.78 GB of model weights for GPT-2, or more than **140x** our storage cost, while still incurring statistical error.

	ResNet-50 $b = 32$	**ResNet-50** $b = 26$	**GPT-2** $b = 32$	**GPT-2** $b = 26$
Naive Encoding	456 MB	456 MB	92 MB	92 MB
Efficient Encoding	105 MB	105 MB	22 MB	22 MB
+ Zip Compression	96 MB	91 MB	20 MB	18 MB

4). We observe that smaller values of b do allow more log entries to be ignored, improving compression of the file, which we discuss next.

Compression with adaptive threshold: Our approach outperforms (Table 1) the storage costs of proof-of-learning protocols that save model weights for GPT-2 (2.78GB), which has many linear layers – we observe more than **140x** reduction relative to the approach in Jia et al. (2021). We further reduce the storage cost of our method by decreasing the rounding amount b and implementing the adaptive thresholding strategy (Section 5.4). Table 3 reports adaptive thresholds τ for four different pytorch layers at rounding amount $b_r = 32$. Convolutions require the lowest τ, indicating larger divergence in outputs between GPU types, which is expected due to the large # of matrix multiplications. Meanwhile, τ is higher for normalization layers, likely due to smaller divergences between GPU types. Because adaptive thresholding seeks to reduce the # of times rounding decisions (0 and 2) are logged and improve log file compression, we report storage cost after zip compression in Table 1. As expected, more aggressive rounding (which results in a higher τ) improves the compression rate. Although the compression gains are mild in comparison to our encoding step, they build-up over the course of training. Finally, we report the average # of rev corrections an auditor needs to perform for one training step in our two tasks (Table 2). These values are surprisingly small in comparison to the # of operations logged – only a maximum of **2e-6%** (ResNet-50) and **9e-6%** (GPT-2) of logged values, are actually needed by the auditor! We also observe that severe rounding (e.g., $b = 27$) completely eliminated the hardware non-determinism for our tasks, requiring no corrections from the auditor. This shows a huge gap between the # of values currently saved by the trainer and those needed by the auditor, motivating an exciting future possibility of significantly reducing the storage cost of our method if we could reliably predict when a divergence will not occur.

6.2. Comparison with alternative approaches

Logistic Regression: Garg et al. (2023) recently proposed a zero-knowledge proof-based system for verifiable training of a logistic regression, which importantly does not leak information about the client's data or require a trusted third-party auditor, unlike our work. However, since verifiable training itself is motivated by a client not having sufficient resources to train the model, it is crucial to consider the implications of scale. The authors report the prover time and proof size requirements for one training pass of logistic regression on a dataset of 2^{18} items, with 1024 dimensions and a batch size of 2014, as **72 seconds** (training and proof generation time) and **350 MB** respectively. We replicate this training task, and find that our method significantly improves upon both storage and time requirements, requiring only **106 KB** and **7 seconds** (both training and auditing). Furthermore, because Garg et al. (2023) do not report the duration of "offline phase" of their method, their reported value is a lower bound on the actual time required. Finally, we note that the original proof-of-learning protocol from Jia et al. (2021), which also considers a trusted third-party, would require **9.2 MB per training step** to store all model weights. Our method is at least **85x** more space efficient.

VGG-11: Concurrent to this work, Abbaszadeh et al. (2024) introduce a zero-knowledge proof-of-training protocol for deep neural networks, presenting results for one batch step

Table 2. Average # of rev corrections performed by auditor per training step. Even at $b = 32$, auditing only requires 20-25 corrections (**2e-6 to 9e-6%** of samples) per training step.

ResNet-50	$b = 32$	$b = 31$	$b = 30$	$b = 29$	$b = 28$	$b = 27$	$b = 26$
Forward	15 ± 3	6 ± 2	3 ± 1	3 ± 1	0	0	0
Backward	10 ± 0.6	6 ± 0.6	2 ± 1	0.7 ± 0.7	0 ± 0	0 ± 0	0 ± 0

GPT-2	$b = 32$	$b = 31$	$b = 30$	$b = 29$	$b = 28$	$b = 27$	$b = 26$
Forward	2 ± 0.7	2.3 ± 0.8	2.2 ± 0.4	0.2 ± 0.2	0.4 ± 0.2	0 ± 0	0 ± 0
Backward	19 ± 13	0.75 ± 0.3	1.2 ± 0.4	0.2 ± 0.2	$0. \pm 0.0$	0 ± 0	0 ± 0

Table 3. Adaptive thresholds identified for different operations using Algorithm 3 with $b = 32$.

	2D Convolution	**Batch Norm**	**Linear**	**Layer Norm**
Dimension	*256 (1,1)*	*(128, 128, 16, 16)*	*(768,768)*	*(768,1)*
τ	$0.305 * 2^{-23}$	$0.499 * 2^{-23}$	$0.465 * 2^{-23}$	$0.499 * 2^{-23}$

of training for a simplified version of the VGG-11 model with 10M parameters, which is less than the original VGG-11 network and ResNet-50 (Simonyan & Zisserman, 2015). While the authors do not provide architectural details, we can assume that increasing the # of parameters to the original VGG-11 would only increase their reported proof time and size. We compare their reported values with an implementation of our method for the same task of verifying the training of VGG-11 on CIFAR-10 with a batch size of 16. While their use of incrementally verifiable computation leads to tractable proof size (1.36MB vs. the 1.2MB per iteration cost of our method), Abbaszadeh et al. (2024)'s method requires **22 min. per training iteration**. In comparison, our method requires training and auditing times of only 6 sec. per iteration and is significantly more efficient (factor of **220x**), an important consideration for commercial FM training. While proof-based systems do not require a third party, they do so at the cost of relying on hard-to-scale cryptographic techniques, as well as approximating non-linear functions that can harm performance.

7. Security Analysis

Our work makes a *1-of-n* honesty assumption, i.e., as long as one of n auditors is honest, any attack from a malicious trainer that results in diverging model weights will be detected. One consideration is the potential manipulation of the rounding logs by an adversarial trainer who could select rounding decisions that achieve a desired outcome, and which the auditor would follow. Concretely, let us define our threat model so that the trainer knows an auditor's GPU a priori. Recall that an auditor only copies the trainer's rounding decision in Case A in Figure 3, when both GPUs compute values close to the rounding boundary. Under this threat model, the trainer can identify the n steps where the auditor is close to the boundary (as in Case A), enumerate the set of 2^n different models that result from different rounding decisions, and selectively pick a model that exhibits a desired property.

However, the trainer cannot use this strategy to embed an arbitrary property (e.g., a specific backdoor). It can only select from the set of models that differ in certain rounding decisions, which all require the trainer to use the correct training specifications accepted by the client (such as exact training data & hyperparameters). Furthermore, since the expected # of divergences between the trainer and the auditor is extremely small (see Table 2), the set of possible models where an auditor would not detect an attack (e.g., many rev ops) is limited. Finally, we show in Table 5 in the appendix that the divergence (measured both as ℓ_2-norm between model weights and output distributions) due to GPU non-determinism is significantly less than the divergence due to data ordering during training. Therefore, if we a client will accept a model trained with *any* random ordering of the data during training, then it is unlikely that an adversarial trainer — that can only alter rounding decisions — could produce a model that the client would not accept. Fully understanding the properties obtained by manipulating logs adversarially is an important future direction.

8. Limitations and Future Work

Our efficient verifiable training scheme successfully controls for hardware nondeterminism. It expands the pool of potential auditors of a model training service, allowing us to envision a world where a client can even use two competing service providers it trusts to audit each other. Relative to proof-based systems, a limitation is the need for all parties to trust the third-party auditor. If the trainer provides finetuning services on top of closed-source models (e.g., OpenAI), then our scheme will only work for the third-party auditors that the trainer is willing to share model weights with. Other limitations included the added latency of training in higher precision and the storage cost. While we have shown that our method requires significantly less storage than alternatives, the vast majority of stored rounding decisions are not used by the auditor and are therefore unnecessary (Section 6). Therefore, an exciting direction for future work is to mitigate this gap by better predicting when GPU divergence between computations occurs via stronger noise profiling (Fang et al., 2023). Finally, another direction for future work also includes adapting our method for distributed training.

References

Abbaszadeh, K., Pappas, C., Papadopoulos, D., and Katz, J. Zero-knowledge proofs of training for deep neural networks. Cryptology ePrint Archive, Paper 2024/162, 2024. URL https://eprint.iacr.org/2024/162. https://eprint.iacr.org/2024/162.

Ames, S., Hazay, C., Ishai, Y., and Venkitasubramaniam, M. Ligero: Lightweight sublinear arguments without a trusted setup. Cryptology ePrint Archive, Paper 2022/1608, 2022. URL https://eprint.iacr.org/2022/1608. https://eprint.iacr.org/2022/1608.

Bitansky, N., Canetti, R., Chiesa, A., and Tromer, E. From extractable collision resistance to succinct non-interactive arguments of knowledge, and back again. In *Innovations in Theoretical Computer Science (ITCS)*, pp. 326–349. ACM, 2012.

Bulck, J. V., Minkin, M., Weisse, O., Genkin, D., Kasikci, B., Piessens, F., Silberstein, M., Wenisch, T. F., Yarom, Y., and Strackx, R. Foreshadow: Extracting the keys to the intel SGX kingdom with transient Out-of-Order execution. In *27th USENIX Security Symposium (USENIX Security 18)*, pp. 991–1008, Baltimore, MD, August 2018. USENIX Association. ISBN 978-1-939133-04-5. URL https://www.usenix.org/conference/usenixsecurity18/presentation/bulck.

Carlini, N., Jagielski, M., Choquette-Choo, C. A., Paleka, D., Pearce, W., Anderson, H., Terzis, A., Thomas, K., and Tramèr, F. Poisoning web-scale training datasets is practical, 2023.

Choi, D., Shavit, Y., and Duvenaud, D. Tools for verifying neural models' training data. In *Neural Information Processing Systems*, 2023.

Chou, Y. H., Ng, C., Cattell, S., Intan, J., Sinclair, M. D., Devietti, J., Rogers, T. G., and Aamodt, T. M. Deterministic atomic buffering. In *2020 53rd Annual IEEE/ACM International Symposium on Microarchitecture (MICRO)*, 2020.

Crane, M. Questionable answers in question answering research: Reproducibility and variability of published results. *Transactions of the Association for Computational Linguistics*, 6:241–252, 2018a. doi: 10.1162/tacl_a_00018. URL https://aclanthology.org/Q18-1018.

Crane, M. Questionable answers in question answering research: Reproducibility and variability of published results. *Transactions of the Association for Computational Linguistics*, 6:241–252, 2018b. doi: 10.1162/tacl_a_00018. URL https://aclanthology.org/Q18-1018.

Defour, D. and Collange, C. Reproducible floating-point atomic addition in data-parallel environment. In *Proc. of the Federated Conference on Computer Science and Information Systems*, 2015.

Dhanuskodi, G., Guha, S., Krishnan, V., Manjunatha, A., Nertney, R., O'Connor, M., and Rogers, P. Creating the first confidential gpus. *Commun. ACM*, 67(1):60–67, dec 2023. ISSN 0001-0782. doi: 10.1145/3626827. URL https://doi.org/10.1145/3626827.

Fang, C., Jia, H., Thudi, A., Yaghini, M., Choquette-Choo, C. A., Dullerud, N., Chandrasekaran, V., and Papernot, N. Proof-of-learning is currently more broken than you think, 2023.

Garg, S., Goel, A., Jha, S., Mahloujifar, S., Mahmoody, M., Policharla, G.-V., and Wang, M. Experimenting with zero-knowledge proofs of training. Cryptology ePrint Archive, Paper 2023/1345, 2023. URL https://eprint.iacr.org/2023/1345. https://eprint.iacr.org/2023/1345.

Goldwasser, S., Kim, M. P., Vaikuntanathan, V., and Zamir, O. Planting undetectable backdoors in machine learning models, 2022.

Gupta, K., Jawalkar, N., Mukherjee, A., Chandran, N., Gupta, D., Panwar, A., and Sharma, R. Sigma: Secure gpt inference with function secret sharing. Cryptology ePrint Archive, Paper 2023/1269, 2023. URL https://eprint.iacr.org/2023/1269. https://eprint.iacr.org/2023/1269.

Jia, H., Yaghini, M., Choquette-Choo, C. A., Dullerud, N., Thudi, A., Chandrasekaran, V., and Papernot, N. Proof-of-learning: Definitions and practice. *CoRR*, abs/2103.05633, 2021. URL https://arxiv.org/abs/2103.05633.

Jooybar, H., Fung, W. W. L., O'Connor, M., Devietti, J., and Aamodt, T. M. Gpudet: a deterministic gpu architecture. In *ASPLOS '13: Proceedings of the eighteenth international conference on Architectural support for programming languages and operating systems*, 2013.

Kahan, W. Further remarks on reducing truncation errors, 1965. URL https://dl.acm.org/doi/pdf/10.1145/363707.363723.

Kang, D., Hashimoto, T., Stoica, I., and Sun, Y. Scaling up trustless dnn inference with zero-knowledge proofs, 2022.

Koh, P. W., Steinhardt, J., and Liang, P. Stronger data poisoning attacks break data sanitization defenses, 2021.

Kong, Z., Chowdhury, A. R., and Chaudhuri, K. Can membership inferencing be refuted?, 2023.

Lee, S., Ko, H., Kim, J., and Oh, H. vcnn: Verifiable convolutional neural network based on zk-snarks. Cryptology ePrint Archive, Paper 2020/584, 2020. URL https://eprint.iacr.org/2020/584. https://eprint.iacr.org/2020/584.

Liu, T., Xie, X., and Zhang, Y. zkcnn: Zero knowledge proofs for convolutional neural network predictions and accuracy. Cryptology ePrint Archive, Paper 2021/673, 2021. URL https://eprint.iacr.org/2021/673. https://eprint.iacr.org/2021/673.

Merkle, R. C. A digital signature based on a conventional encryption function. In Pomerance, C. (ed.), *Advances in Cryptology — CRYPTO '87*, pp. 369–378, Berlin, Heidelberg, 1988. Springer Berlin Heidelberg. ISBN 978-3-540-48184-3.

Micali, S. CS proofs (extended abstracts). In *35th Annual Symposium on Foundations of Computer Science, Santa Fe, New Mexico, USA, 20-22 November 1994*, pp. 436–453. IEEE Computer Society, 1994. doi: 10.1109/SFCS.1994.365746. URL https://doi.org/10.1109/SFCS.1994.365746.

Nilsson, A., Bideh, P. N., and Brorsson, J. A survey of published attacks on intel sgx, 2020.

NVIDIA. Determinism across gpu architectures, 2022. URL https://github.com/NVIDIA/framework-reproducibility/issues/28.

NVIDIA. Cuda: Hopper tuning guide, 2023. URL https://docs.nvidia.com/cuda/pdf/Hopper_Tuning_Guide.pdf.

Sevilla, J., Heim, L., Ho, A., Besiroglu, T., Hobbhahn, M., and Villalobos, P. Compute trends across three eras of machine learning. In *2022 International Joint Conference on Neural Networks (IJCNN)*. IEEE, July 2022. doi: 10.1109/ijcnn55064.2022.9891914. URL http://dx.doi.org/10.1109/IJCNN55064.2022.9891914.

Simonyan, K. and Zisserman, A. Very deep convolutional networks for large-scale image recognition, 2015.

Srivastava, M., Nushi, B., Kamar, E., Shah, S., and Horvitz, E. An empirical analysis of backward compatibility in machine learning systems, 2020.

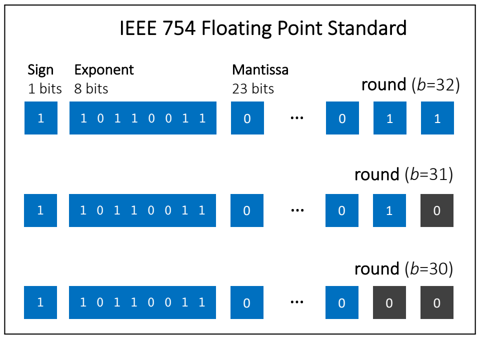

Figure 5. We define rounding to b bits as rounding to the nearest 32-bit FP number that has 0s in the last $32 - b$ bits of the mantissa, after accounting for the exponent.

TensorFlow. Tensorflow 2.8.0-rc0, 2021. URL https://github.com/tensorflow/tensorflow/releases/tag/v2.8.0-rc0.

Teutsch, J. and Reitwießner, C. A scalable verification solution for blockchains. *CoRR*, abs/1908.04756, 2019. URL http://arxiv.org/abs/1908.04756.

Thudi, A., Jia, H., Shumailov, I., and Papernot, N. On the necessity of auditable algorithmic definitions for machine unlearning. In *31st USENIX Security Symposium (USENIX Security 22)*, pp. 4007–4022, Boston, MA, August 2022. USENIX Association. ISBN 978-1-939133-31-1. URL https://www.usenix.org/conference/usenixsecurity22/presentation/thudi.

Wan, A., Wallace, E., Shen, S., and Klein, D. Poisoning language models during instruction tuning, 2023.

Whitehead, N. and Fit-Florea, A. Precision & performance: Floating point and ieee 754 compliance for nvidia gpus, 2011. URL https://developer.nvidia.com/sites/default/files/akamai/cuda/files/NVIDIA-CUDA-Floating-Point.pdf.

Zhuang, D., Zhang, X., Song, S. L., and Hooker, S. Randomness in neural network training: Characterizing the impact of tooling. In *arXiv:2106.11872v1*, 2021.

A. IEEE Floating Point Image

See Figure 5.

B. GPU Details

All experiments reported in our paper are run with the following three GPUs:

- NVIDIA Titan XP: 3840 Cores, 12 GB
- NVIDIA RTX 2080 Ti: 4352 Cores, 11 GB
- NVIDIA A40: 10752 Cores, 48 GB

We are able to successfully replicate training runs between all pairs of these 3 GPUs.

C. Logging Algorithm

See Algorithm 4

D. Train Algorithm

See Algorithm 1.

E. Audit Algorithm

See Algorithm 2.

F. Adaptive Thresholding Algorithm

See Algorithm 3.

G. Time Requirements

See Table 4.

H. Model Divergence Comparison

See Table 5.

I. Random Number Generation

Our verifiable training scheme requires shared randomness between the trainer and auditor, which is used for deciding input data batching, weight initialization, and operations such as dropout (randomly setting outputs to zero). More formally, our scheme requires sharing the same random seed and pseudo-random generator. However, in our implementation based on `pytorch` (assuming the same software version between trainer and auditor), we chose to rely on the the `torch` random seed functionality. While this successfully controls for batch input ordering and weight initialization, it is unfortunately not sufficient for random number generation, as operations such as `torch.nn.randn()` leverage parallelism when the requested # of values is higher than a certain amount. Specifically, we found that across T40, RTX 2080 Ti, V100, A40, and A100, given the same seed, torch.randint() produces identical tensors onlt up to size 40960. At size 40961, T40 (which is an older GPU) deviated from the rest. Likewise, at size 69633, 2080 Ti deviated from the rest, and so on. Based on these observations, we arranged for calls to torch.randint() in the dropout layer (which is the only operation using large random tensors in our tasks) to be replaced by generating and concatenating multiple random tensors of size 40960 or less. Specifically, a random tensor of size $n > 40960$ is generated by concatenating $(n//40960)$ random tensors of size 40960 and one random tensor of size $(n\%40960)$. However, we emphasize that it is therefore important in our scheme either for both parties to implement this change a priori, or simply use an external source for pseudorandomness.

Algorithm 1 train

INPUT: dataset D, epochs E, batch size B, shared randomness R, model W_θ, loss function loss, rounding amount b_r, training precision b_{tr}, target model precision b_m, checkpointing interval k
OUTPUT: Merkle tree root M_{root}, rounding log file F

```
1: $F, M_{leaves} \leftarrow$ create empty file and leaf list
2: $W_\theta \leftarrow \mathsf{init}(R, b_{tr})$ //initialize weights
3: $T \leftarrow \frac{D*E}{B}$
4: for $t = 1...T$ do
5:     $input \leftarrow \mathsf{batch}(R, D, B)$ // get data batch
       // forward pass
6:     for layer $l_\theta \in W_\theta$.layers do
7:         $output \leftarrow l_\theta(input)$
8:         $\tau \leftarrow \mathsf{threshold}(l_\theta, b_r, b_{tr})$ //set threshold
9:         $\mathsf{log}(output, b_r, \tau, F)$
10:        $output \leftarrow \mathsf{rnd}_{b_r}(output)$
11:        $input \leftarrow output$
12:    end for
13:    $loss \leftarrow \mathsf{loss}(output)$
14:    // backward pass, reversed layers
15:    $grad\_output \leftarrow \nabla_{\mathsf{loss}}$
16:    for layer $l_\theta \in W_\theta$.layers do
17:        $grad\_input \leftarrow \nabla_{l_\theta}(grad\_output)$
18:        $\tau \leftarrow \mathsf{threshold}(\nabla_{l_\theta}, b_r, b_{tr})$
19:        $\mathsf{log}(grad\_input, b_r, \tau, F)$
20:        $grad\_input \leftarrow \mathsf{rnd}_{b_r}(grad\_input)$
21:        $grad\_output \leftarrow grad\_input$
22:    end for
23:    $\theta \leftarrow$ update update weights
24:    if $t$ mod $k = 0$ then
25:        $M_{leaves}$.append(hash$_{\mathsf{sha256}}$($\theta$ in precision $b_m$))
26:    end if
27: end for
28: $M_{root} \leftarrow \mathsf{tree}(M_{leaves})$ // create Merkle tree
29: return $F, M_{root}$, and model $W_\theta$ in target precision $b_m$
```

Algorithm 2 audit

```
INPUT: dataset $D$, epochs $E$, batch size $B$, shared randomness $R$, model $W_\theta$, loss function loss, rounding amount $b_r$, training precision $b_{tr}$, target model precision $b_m$, checkpointing interval $k$, log file $F$ from trainer
OUTPUT: Merkle tree root $M_{root}$

1: $M_{leaves} \leftarrow$ create empty leaf list
2: $W_\theta \leftarrow \mathsf{init}(R, b_{tr})$ //initialize weights
3: $T \leftarrow \frac{D*E}{B}$
4: for $t = 1 ... T$ do
5:   $input \leftarrow \mathsf{batch}(R, D, B)$ // get data batch
     // forward pass
6:   for layer $l_\theta \in W_\theta$.layers do
7:     $output \leftarrow l_\theta(input)$
8:     for $output_i \in output$ do
9:       // Match trainer rounding
10:      $c \leftarrow \mathsf{read}(output_i, F)$
11:      $output_i \leftarrow \mathsf{rev}(output_i, b_r, c)$
12:    end for
13:    $input \leftarrow output$
14:  end for
15:  $loss \leftarrow \mathsf{loss}(output)$
16:  // backward pass
17:  $grad\_output \leftarrow \nabla_{\mathsf{loss}}$
18:  for layer $l_\theta \in W_\theta$.layers do
19:    $grad\_input \leftarrow \nabla_{l_\theta}(grad\_output)$
20:    for $grad\_input_i \in grad\_input$ do
21:      // Match trainer rounding
22:      $c \leftarrow \mathsf{read}(grad\_input_i, F)$
23:      $grad\_input_i \leftarrow \mathsf{rev}(grad\_input_i, b_r, c)$
24:    end for
25:    $grad\_output \leftarrow grad\_input$
26:  end for
27:  $\theta \leftarrow$ update update weights
28:  if $t$ mod $k = 0$ then
29:    $M_{leaves}.\mathsf{append}(\mathsf{hash}_{\mathsf{sha256}}(\theta$ in precision $b_m))$
30:  end if
31: end for
32: $M_{root} \leftarrow \mathsf{tree}(M_{leaves})$ // create Merkle tree
33: return $M_{root}$
```

Algorithm 3 threshold

```
INPUT: layer $l$, rounding amount $b_r$, training precision $b_{tr}$
OUTPUT: threshold $\tau$
1: $P \leftarrow$ initialize empty list
2: $N, T \leftarrow$ initialize large # of data points and iterations
3: for i=1...N do
4:   $GPU1, GPU2 \leftarrow$ select two different GPU architectures
5:   $x \leftarrow$ select random input for layer $l$ in $b_{tr}$ floating-point precision
6:   $y_1 \leftarrow l_{GPU1}(x), y_2 \leftarrow l_{GPU2}(x)$, apply layer $l$ on input $x$ on each GPU
7:   if $\mathsf{rnd}_{b_r}(y_1) \neq \mathsf{rnd}_{b_r}(y_2)$ then
8:     if $y_1 > \mathsf{rnd}_{b_r}(y_1)$ and $y_2 < \mathsf{rnd}_{b_r}(y_2)$ then
9:       $P.\mathsf{append}(|y_1 - \mathsf{rnd}_{b_r}(y_1)|)$
10:      $P.\mathsf{append}(|y_2 - \mathsf{rnd}_{b_r}(y_2)|)$
11:    end if
12:    if $y_1 < \mathsf{rnd}_{b_r}(y_1)$ and $y_2 > \mathsf{rnd}_{b_r}(y_2)$ then
13:      $P.\mathsf{append}(|y_1 - \mathsf{rnd}_{b_r}(y_1)|)$
14:      $P.\mathsf{append}(|y_2 - \mathsf{rnd}_{b_r}(y_2)|)$
15:    end if
16:  end if
17: end for
18: //binary search to select threshold
19: $lower, upper, \tau \leftarrow 0.25 * (2^{-23}), 0.5 * (2^{9-b_r}), 0$
20: for t=1...T do
21:   $\tau \leftarrow (lower + upper)/2$
22:   $success \leftarrow True$
23:   for $p_i \in P$ do
24:     exp $\leftarrow$get exponent of $p_i$
25:     if $p_i <$ exp $*\tau$ then
26:       $success \leftarrow False$
27:     end if
28:   end for
29:   if $success$ then
30:     $lower \leftarrow \tau$
31:   else
32:     $upper \leftarrow \tau$
33:   end if
34: end for
35: return $\tau$
```

Algorithm 4 log

INPUT: value x, rounding amount b_r, threshold τ, file F

```
1: $\exp \leftarrow$ get exponent of $x$
2: if $|x - \mathsf{rnd}_{b_r}(x)| > \exp * \tau$ and $x < \mathsf{rnd}_{b_r}(x)$ then
3:     $\mathsf{write}(2, F)$ // log rounding up
4: else if $|x - \mathsf{rnd}_{b_r}(x)| > \exp * \tau$ and $x > \mathsf{rnd}_{b_r}(x)$ then
5:     $\mathsf{write}(0, F)$ // log rounding down
6: else
7:     $\mathsf{write}(1, F)$ // log rounding ignore
8: end if
```

J. Comparison with GPT-2 Inference

The previously discussed proof-based systems for verifiable training by-pass the need for a third-party auditor, but very few efficient systems exist in the literature. Many more works study secure *inference* of deep neural networks, which could be used to construct verifiable training protocols with stronger security guarantees than ours (e.g., allowing a trainer to keep a proprietary model's weights private), but come at a significant cost to performance and resources. To demonstrate this, we consider adapting Gupta et al. (2023)'s protocol for secure inference of GPT-2 based on multi-party computation, to our context of verifiable training. Gupta et al. (2023) show how two parties, the client with private data and the trainer, can jointly compute the forward pass of a known model architecture without revealing additional information beyond the model output to each other. Because they report the the communication overhead $P = 0.37$GB and time $T = 0.96$ seconds for one forward pass on a single data input, we can calculate $2 \times P \times D \times E =$ **189 GB** and $2 \times T \times D \times E =$ **983 seconds** as estimated communication cost and time, respectively, for 1 step of training in out GPT-2 task, where 2 considers both the forward and backward pass. Compared with our method's required storage cost (18MB) and training time (11s for training, 13.5 seconds for auditing), scaling Gupta et al. (2023)'s protocol for training would introduce around a **10,000x** data and **40x** time overhead.

Table 4. Training time requirements, including Merkle tree operations (at $k = 5$), for 1 step of training broken down by stage of our verifiable training process. Note that reported times are specific to the particular dataset, batch size, and task, and using a non-optimized prototype codebase – therefore the relative increase is time is more important.

	ResNet-50	GPT-2
Original (No Rounding or Disk I/O)	24s	8s
Trainer	28s	11s
Auditor	31s	13.5

Table 5. Comparison of model divergence due to data ordering versus GPU non-determinism. Reported numbers are averaged between 10 pairs of models, error bars are standard deviation.

Metric	Data Ordering	GPU Non-determinism
l2 weight difference	133.2 ± 9	1.1 ± 0.07
l2 output distance	5.3 ± 0.03	0.26 ± 0.02